Inorganic Chemistry

Article

pubs.acs.org/IC

Mesityltellurenyl Cations Stabilized by Triphenylpnictogens $[MesTe(EPh_3)]^+$ (E = P, As, Sb)†

Jens Beckmann,*[‡,§] Jens Bolsinger,[§] Andrew Duthie,[⊥] Pamela Finke,[‡,§] Enno Lork,[‡] Carsten Lüdtke,[§] Ole Mallow,[‡,§] and Stefan Mebs*[§]

[‡]Institut für Anorganische und Physikalische Chemie, Universität Bremen, Leobener Strasse, D-28359 Bremen, Germany

[§]Institut für Chemie und Biochemie, Freie Universität Berlin, Fabeckstrasse 34/36, D-14195 Berlin, Germany

[⊥]School of Life and Environmental Sciences, Deakin University, Pigdons Road, Waurn Ponds 3217, Australia

Supporting Information

ABSTRACT: The homoleptic 1:1 Lewis pair (LP) complex $[MesTe(TeMes_2)]O_3SCF_3$ (**1**) featuring the cation $[MesTe(TeMes_2)]^+$ (**1a**) was obtained by the reaction of Mes_2Te with HO_3SCF_3. The reaction of **1** with Ph_3E (E = P, As, Sb, Bi) proceeded with substitution of Mes_2Te and provided the heteroleptic 1:1 LP complexes $[MesTe(EPh_3)]O_3SCF_3$ (**2**, E = P; **3**, E = As) and $[MesTe(SbPh_3)][Ph_2Sb(O_3SCF_3)_2]$ (**4**) featuring the cations $[MesTe(EPh_3)]^+$ (**2a**, E = P; **3a**, E = As; **4a**, E = Sb) and the anion $[Ph_2Sb(O_3SCF_3)_2]^-$ (**4b**). In the reaction with Ph_3Bi, the crude product contained the cation $[MesTe(BiPh_3)]^+$ (**5a**) and the anion $[Ph_2Bi(O_3SCF_3)_2]^-$ (**5b**); however, the heteroleptic 1:1 LP complex $[MesTe(BiPh_3)][Ph_2Bi(O_3SCF_3)_2]$ (**5**) could not be isolated because of its limited stability. Instead, fractional crystallization furnished a large amount of $Ph_2BiO_3SCF_3$ (**6**), which was also obtained by the reaction of Ph_3Bi with HO_3SCF_3. The formation of the anions **4b** and **5b** involves a phenyl group migration from Ph_3E (E = Sb, Bi) to the $MesTe^+$ cation and afforded MesTePh as the byproduct, which was identified in the mother liquor. The heteroleptic 1:1 LP complexes **2**–**4** were also obtained by the one-pot reaction of Mes_2Te, Ph_3E (E = P, As, Sb) and HO_3SCF_3. Compounds **1**–**4** and **6** were investigated by single-crystal X-ray diffraction. The molecular structures of **1a**–**4a** were used for density functional theory calculations at the B3PW91/TZ level of theory and studied using natural bond order (NBO) analyses as well as real-space bonding descriptors derived from an atoms-in-molecules (AIM) analysis of the theoretically obtained electron density. Additionally, the electron localizability indicator (ELI-D) and the delocalization index are derived from the corresponding pair density.

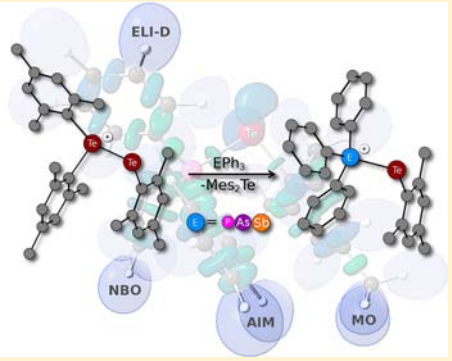

INTRODUCTION

Like silylenes (R_2Si), the isoelectronic phosphenium cations (R_2P^+) and sulfonium dications (R_2S^{2+}) as well as their heavier congeners are unsaturated (six-valence-electron) species possessing a vacant p orbital and one lone pair and accordingly may react as Lewis acid and base. Phosphenium cations can be stabilized using strong σ-donor ligands, such as phosphines and N-heterocyclic carbenes (NHCs), as exemplified by the 1:1 Lewis pair (LP) complexes $[Ph_2P(PPh_3)]O_3SCF_3$[1] and $[Ph_2P(CR_2)]AlCl_4$ (CR_2 = 1,3-diisopropyl-4,5-dimethylimidazol-2-ylidene).[2] For related arsenium (R_2As^+), stibenium (R_2Sb^+), and bismuthenium (R_2Bi^+) cations, similar homoleptic 1:1 complexes, e.g., $[PhMeAs(AsPh_3)]O_3SCF_3$,[3] and $[Me_2Sb(SbMe_3)]MeSbBr_3$,[4] and heteroleptic 1:1 LP complexes, e.g., $[Ph_2E(PPh_3)]PF_6$ (E = As, Sb, Bi),[5−8] were reported. For the heavier pnictogens, also 1:2 LP complexes, e.g., $[Ph_2E(PPh_3)_2]PF_6$ (E = Sb, Bi), were described.[5−8] For $[Ph_2E(PPh_3)_n]^+$ (n = 1, 2), the bonding situation was investigated in terms of bond dissociation energies, bond decomposition, and molecular orbital (MO) analyses.[8] The first highly charged chalcogen(IV) dications were stabilized by intramolecularly coordinating pincer ligands featuring S donor atoms.[9] More recently, highly charged chalcogen(II) dications were obtained by the reaction of in situ generated chalcogen(II) triflates with 1,4-diaryl-1,4-diaza-1,3-butadiene (R_2DAB) ligands, diiminopyridine (R_2DIMPY) ligands, bis(arylimino)acenaphthene (R_2BIAN) ligands, two monodentate pyridines, two NHCs, and chelating bis(phosphino) and bis(arsino) ligands.[10]

Tellurenyl ions (RTe^+) are unsaturated (six-valence-electron) species having not only a vacant p orbital but also two lone pairs, which raises the prospect of an interesting reactivity.

There have been a number of reports on intramolecularly[11,12] and intermolecularly[13−21] σ-donor-stabilized tellurenyl cations. The fully characterized di- and trinuclear tellurium compounds $[MesTe(TeMes_2)_n]SbF_6$ (n = 1, 2) were regarded as homoleptic 1:1 and 1:2 LP complexes of the mesityltellurenyl cation $MesTe^+$ and the Lewis base Mes_2Te (Mes = 2,4,6-$Me_3C_6H_2$).[13,14] Mesityltellurenyl cations stabilized by trialkyl-

Received: August 13, 2012
Published: November 7, 2012

   dx.doi.org/10.1021/ic3017722 | Inorg. Chem. 2012, 51, 12395−12406

phosphine selenides $[MesTe(SeP\text{-}t\text{-}Bu_2\text{-}i\text{-}Pr)_n]SbF_6$ (n = 1, 2) were characterized by multinuclear NMR spectroscopy, but no structural information was disclosed.[14] A similar 4-tolyltellurenyl cation stabilized by a trialkylphosphine selenide, $[4\text{-}MeC_6H_4Te(SeP\text{-}t\text{-}Bu\text{-}i\text{-}Pr_2)]4\text{-}MeC_6H_4TeI_2$ was claimed; however, because of the short Te−Te interaction, this compound might be better viewed as a σ-donor-stabilized mixed-valent 4-tolyltellurenyl halide $[(t\text{-}Bu\text{-}i\text{-}Pr_2PSe)(4\text{-}MeC_6H_4)TeTeI_2(4\text{-}MeC_6H_4)]$.[15] Previously, two tributylphosphine-stabilized organotellurenyl cations, $[4\text{-}FC_6H_4Te(PBu_3)]BF_4$ and $[MeTe(PBu_3)]ClO_4$, were obtained as oils and characterized only tentatively by ^{31}P and ^{125}Te NMR spectroscopy,[16] whereas the lighter organochalcogenyl(II) cations were already known, as exemplified by the fully characterized perchlorate salts $[PhS(PPh_3)]ClO_4$[17] and $[MeSe(PPh_3)]ClO_4$.[18] The lack of structural information on tellurenyl cations stabilized by strong σ donor atoms prompted us to investigate phosphine and NHC complexes in more detail. In preceding work, we already described the NHC-stabilized *m*-terphenyltellurenyl cation $[2,6\text{-}Mes_2C_6H_3Te(CR_2)]X$ (X = 2,6-$Mes_2C_6H_3TeCl_2$, 2,6-$Mes_2C_6H_3TeBr_2$, I; CR_2 = 1,3,4,5-tetramethylimidazole-2-ylidene) that was prepared starting from the (mixed-valent) *m*-terphenyltellurenyl halides $(2,6\text{-}Mes_2C_6H_3)TeTeX_2(2,6\text{-}Mes_2C_6H_3)$ (X = Cl, Br) and 2,6-$Mes_2C_6H_3TeI$.[19] Complementing the experimental work, we also disclosed calculated gas-phase structures, dissociation energies, and the results of natural bond order (NBO) analyses of NHC- and phosphine-stabilized phenyltellurenyl cations $[PhTe(CR_2)]^+$ and $[PhTe(PMe_3)]^+$ (CR_2 = 1,3,4,5-tetramethylimidazol-2-ylidene).[19] During the course of this work, aryltellurenyl cations were trapped using acetylenes, affording tellurenium ions $[RTe(CR')_2]^+$.[20] The lighter thiiranium and seleniranium ions $[RE(CR')_2]^+$ (E = S, Se) were already previously known and have recently attracted considerable attention in organic syntheses.[21] Very recently, aryltellurenyl cations were also trapped using butadienes, giving rise to the formation of telluronium ions incorporated into cyclopropenes.[22] In the latter report, the first fully characterized phosphine-stabilized aryltellurenyl cations $[BbtTe(PPh_3)]X$ [X = O_3SCF_3, BF_4, $N(O_3SCF_3)_2$; Bbt = 2,6-$\{(Me_3Si)_2CH\}_2$-4-$\{(Me_3Si)_3C\}C_6H_2$] were also described, which have been obtained by the reaction of (mixed-valent) bulky aryltellurenyl halides with triphenylphosphine in the presence of silver salts AgX or trimethylsilanes Me_3SiX.[22]

We have now found a simple and convenient synthetic protocol for preparation of the homoleptic 1:1 LP complex $[MesTe(TeMes_2)]^+$ (**1a**) that readily underwent nucleophilic substitution reactions with triphenylpnictogens Ph_3E (E = P, As, Sb, Bi) to give a series of archetypical σ-donor-stabilized tellurenyl cations $[MesTe(EPh_3)]^+$ (**2a**, E = P; **3a**, E = As; **4a**, E = Sb; **5a**, E = Bi). Density functional theory (DFT) calculations and state-of-the-art analytical methods, including NBO, atom-in-molecules (AIM), and electron localizability indicator (ELI-D), of homo- and heteroleptic 1:1 LP complexes **1a**−**4a** were carried out in an effort to shed some light on the electronic structure and the formal dative Te−E bonds (E = Te, P, As, Sb). Analysis of the Te−E bonds (E = main-group and transition metals) is of substantial current interest because they are prominently featured within metal ditelluroimidodiphosphinates,[23] polyfunctional Lewis acids,[24] and redox-active dinuclear complexes.[25]

RESULTS AND DISCUSSION

The reported homoleptic 1:1 LP complex $[MesTe(TeMes_2)]SbF_6$ was prepared by the reaction of Mes_2Te, MesTeTeMes, Br_2, and $AgSbF_6$ (Mes = 2,4,6-$Me_3C_6H_2$).[13,14] This reaction most likely involves the formation of unstable mesityltellurenyl bromide MesTeBr as the reaction intermediate. We have now found a more straightforward synthetic protocol avoiding the use of bromine and silver salts for the preparation of an analogue, namely, $[MesTe(TeMes_2)]O_3SCF_3$ (**1**) featuring the same cation **1a**. Compound **1** was obtained by the reaction of Mes_2Te with triflic acid in acetonitrile (MeCN) and isolated by crystallization as a brownish dark-red solid in 87% yield (eq 1).

$$2Mes_2Te + HO_3SCF_3 \xrightarrow[-MesH]{} \underset{\mathbf{1}}{[MesTe(TeMes_2)]O_3SCF_3} \quad (1)$$

The mesitylene formed as a side product was removed, together with the solvent from the reaction mixture, by vacuum distillation and identified by NMR spectroscopy. Regardless of whether an excess of triflic acid was applied, the reaction always stopped when half of Mes_2Te was consumed. Apparently, protonation of Mes_2Te produced a (solvated) mesityltellurenyl cation, $MesTe^+$, which immediately formed a 1:1 LP complex with the second half of Mes_2Te. To the best of our knowledge, selective aryl cleavage reactions involving group 16 compounds using triflic acid are unprecedented; however, we are aware that this reaction type is a standard tool for functionalization of group 14 organyls.[26] The reaction mechanism of these cleavage reactions involves an electrophilic ipso substitution at the aromatic ring in which triorganoelement cations R_3E^+ (E = Si, Ge, Sn; R = alkyl, aryl) play an important role. A similar mechanism involving tellurenyl cations RTe^+ may be operative for the reaction of Mes_2Te with triflic acid. Unlike $[MesTe(TeMes_2)]SbF_6$,[13,14] **1** is readily soluble in organic solvents, such as CH_2Cl_2, $CHCl_3$, tetrahydrofuran (THF), and MeCN, thus enabling characterization in solution. The ^{125}Te NMR spectrum ($CDCl_3$) showed two signals at 844.8 ($\omega_{1/2}$ = 293 Hz) and 376.5 ppm with an integral ratio of 1:1, which were unambiguously assigned to the $MesTe^+$ and Mes_2Te moieties, respectively. The assignment was supported by an NMR experiment, in which small amounts of Mes_2Te were successively added to a solution of **1**. Each addition increased the intensity of the signal originally at 376.5 ppm, which was shifted toward the ^{125}Te NMR chemical shift of pure Mes_2Te (250.5 ppm), while the position and intensity of the signal at 844.8 ppm remained almost the same. No evidence was found for the formation of the homoleptic 1:2 LP complex $[MesTe(TeMes_2)_2]O_3SCF_3$. Apparently, the exchange between coordinated and free Mes_2Te is fast on the ^{125}Te NMR time scale. The electrospray ionization mass spectrometry (ESI-MS) spectrum (MeCN, positive detection mode) of **1** revealed only one prominent mass cluster at m/z 617.2 for **1a**. Conductivity measurements confirmed that electrolytic dissociation of **1** into **1a** and triflate ions occurs in solution. The molar conductivity (MeCN, $c = 5 \times 10^{-7}$ mol L^{-1}) of **1** (Λ = 360 Ω^{-1} cm^2 mol^{-1}) is in agreement with the presence of 1:1 electrolytes.[27] The crystal structure of **1** is shown in Figure 1, and selected bond parameters are collected in the caption of the figure.

Similar to $[MesTe(TeMes_2)]SbF_6$, **1** forms a macrocycle comprised of two **1a** cations and two triflate anions, which are associated with secondary Te···O contacts of 2.651(4) and 3.091(5) Å that lie between the sum of covalent radii (2.04 Å)[28] and the sum of van der Waals radii (3.58 Å).[29] In general,

dx.doi.org/10.1021/ic3017722 | Inorg. Chem. 2012, 51, 12395−12406

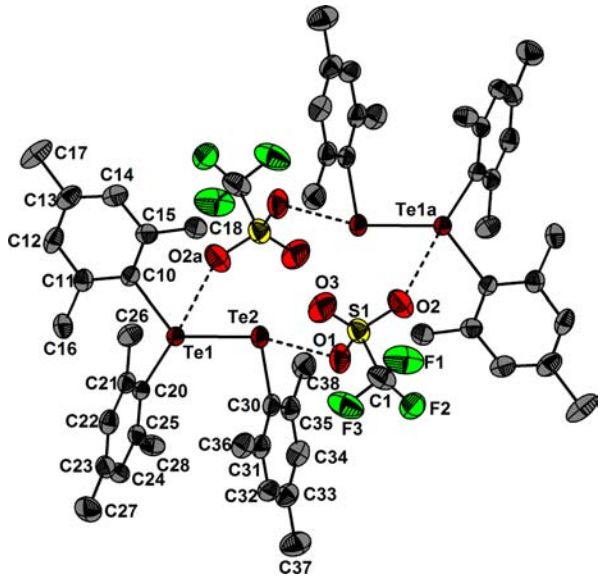

Figure 1. Molecular structure of **1** showing 50% probability ellipsoids and the crystallographic numbering scheme (symmetry code used to generate crystallographically related atoms: a = 2 − *x*, −*y*, −*z*). Selected bond parameters (Å and deg): Te1···O2a 3.091(5), Te1−Te2 2.808(1), Te1−C10 2.127(5), Te1−C20 2.135(5), Te2···O1 2.651(4), Te2−C30 2.134(5); C10−Te1−C20 101.4(2), C10−Te1−Te2 114.4(1), C20−Te1−Te2 94.6(1), C30−Te2−Te1 84.7(1).

the bond parameters of **1a** are very similar in both complexes; however, the Te−Te bond length of **1** [2.808(1) Å] is somewhat longer than that of $[MesTe(TeMes_2)]SbF_6$ [2.7645(5) Å].[13]

It was proposed that $[MesTe(TeMes_2)]SbF_6$ could be of significance for the synthesis of new cationic organotellurium compounds.[13] With this idea in mind, we investigated the reactivity of **1** toward the σ donors Ph_3E (E = P, As, Sb, Bi).

The reaction of **1** with Ph_3P and Ph_3As proceeded with smooth substitution of Mes_2Te, which precipitated from the reaction mixture, providing the heteroleptic 1:1 LP complexes $[MesTe(EPh_3)]O_3SCF_3$ (**2**, E = P; **3**, E = As) featuring the cations $[MesTe(EPh_3)]^+$ (**2a**, E = P; **3a**, E = As). Compounds **2** and **3** were isolated by crystallization as orange solids in 79 and 26% yield (Scheme 1). Notably, **2** and **3** were also prepared by the one-pot reaction of Mes_2Te, Ph_3E (E = P, As), and HO_3SCF_3, albeit in somewhat lower yields.

Scheme 1. Synthesis of 2 and 3

$$[MesTe(TeMes_2)]O_3SCF_3 \xrightarrow[-\ Mes_2Te]{Ph_3E} [MesTe(EPh_3)]O_3SCF_3$$

1 → **2**, E = P; **3**, E = As

$$\text{or}\quad Mes_2Te + HO_3SCF_3 \xrightarrow[-\ MesH]{Ph_3E} [MesTe(EPh_3)]O_3SCF_3$$

Compound **2** is an analogue of the very recently communicated complexes $[BbtTe(PPh_3)]X$ [X = O_3SCF_3, BF_4, $N(O_3SCF_3)_2$] containing a bulkier aryl substituent and different counterions.[22] Compounds **2** and **3** are readily soluble in a number of organic solvents including CH_2Cl_2, $CHCl_3$, THF, and MeCN. The ^{125}Te NMR spectrum ($CDCl_3$) of **2** showed a doublet at 393.0 ppm with a $^1J(^{125}Te-^{31}P)$ coupling of 1148 Hz, whereas the ^{125}Te NMR spectra (CD_3CN) of **2** and **3** exhibited singlets at 385.6 ($\omega_{1/2}$ = 185 Hz) and 408.5 ppm, respectively. These chemical shifts are generally consistent with those reported for $[4\text{-}FC_6H_4Te(PBu_3)]BF_4$ (360 ppm)[16] and $[BbtTe(PPh_3)]O_3SCF_3$ (464 ppm),[22] respectively. The $^1J(^{125}Te-^{31}P)$ coupling constant of **2** compares well with those of $[4\text{-}FC_6H_4Te(PBu_3)]BF_4$ (1071 Hz), $[MeTe(PBu_3)]ClO_4$ (1046 Hz),[16] and $[BbtTe(PPh_3)]O_3SCF_3$ (1387 Hz).[22] The lack of a $^1J(^{125}Te-^{31}P)$ coupling constant in CD_3CN is tentatively attributed to the kinetic lability of **2a** on the NMR time scale. Dissociation and association of Ph_3P may be fast on the NMR time scale in competition with the σ-donor solvent. The ^{31}P NMR spectrum ($CDCl_3$) of **2** showed a singlet at 6.0 ppm, which is significantly shifted from that of free Ph_3P (−4.1 ppm). No evidence was found for the formation of a 1:2 LP complex by NMR spectroscopy. The ^{125}Te NMR chemical shift ($CDCl_3$) remained nearly unchanged when more equivalents of Ph_3P were successively added to a solution of **2**. Upon addition, the ^{31}P NMR signal of **2** shifted toward that of free Ph_3P. The exchange between complexing and free Ph_3P appears to be fast on the NMR time scale. The ^{31}P NMR spectrum (CD_3CN) of **2** displayed a singlet at 4.7 ppm. The fact that the latter value lies between the chemical shifts of **2** in $CDCl_3$ and free Ph_3P tentatively supports the idea that acetonitrile is to some extent a competitive σ donor. The ESI-MS spectra (MeCN, positive detection mode) of **2** and **3** show prominent mass clusters at *m*/*z* 511.1 and 555.2 for **2a** and **3a**, respectively. The molar conductivity (MeCN, $c = 5 \times 10^{-7}$ mol l^{-1}) of **2** (Λ = 400 Ω^{-1} cm^2 mol^{-1}) is consistent with the presence of 1:1 electrolytes.[27] The crystal structures of **2** and **3** are shown in Figures 2 and 3.

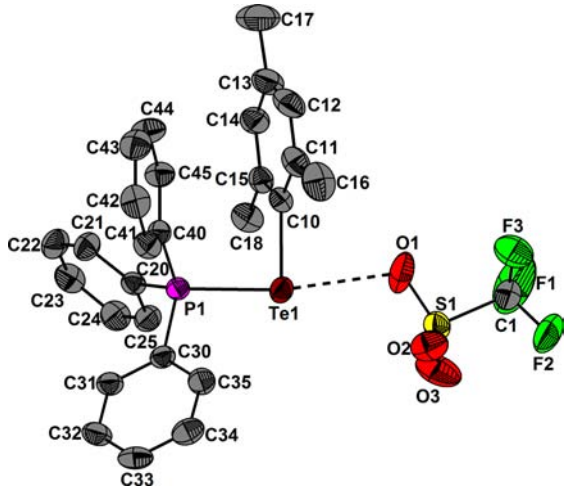

Figure 2. Molecular structure of **2** showing 50% probability ellipsoids and the crystallographic numbering scheme. Selected bond parameters (Å and deg): Te1···O1 2.829(3), Te1−P1 2.467(1), Te1−C10 2.127(3), P1−C20 1.802(3), P1−C30 1.802(3), P1−C40 1.798(3); C10−Te1−P1 91.29(9).

Selected bond parameters of **2** and **3** are collected in the caption of the figures. As in $[BbtTe(PPh_3)]X$ [X = O_3SCF_3, BF_4, $N(O_3SCF_3)_2$], **2** and **3** exhibit T-shaped structures. The Te−E bond lengths of **2** [2.467(1) Å; E = P] and **3** [2.5799(6) Å; E = As] are close to the sum of covalent radii (2.45 Å, E = P; 2.57 Å, E = As)[28] and account for bond orders of about 1. The C−Te−E bond angles of **2** [91.29(9)°, E = P] and **3** [92.10(6)°, E = As] are smaller than that of $[BbtTe(PPh_3)]O_3SCF_3$ [103.25(8)°],[22] presumably because of steric repulsion involving the bulky Bbt substituent in the latter compound. In

dx.doi.org/10.1021/ic3017722 | *Inorg. Chem.* 2012, 51, 12395−12406

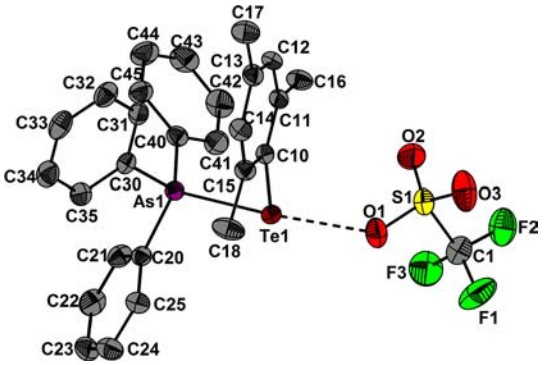

Figure 3. Molecular structure of **3** showing 50% probability ellipsoids and the crystallographic numbering scheme. Selected bond parameters (Å and deg): Te1···O1 2.792(3), Te1−As1 2.5799(6), Te1−C10 2.126(2), As1−C20 1.916(2), As1−C30 1.920(2), As1−C40 1.927(2); C10−Te1−As1 92.10(6).

$[MesTe(EPh_3)]O_3SCF_3$ (**2**, E = P; **3**, E = As), the cations **2a** and **3a** are associated with the triflate anions by secondary Te···O contacts of 2.829(3) and 2.792(3) Å that are shorter than the sum of van der Waals radii (3.58 Å).[29] In $[BbtTe(PPh_3)]O_3SCF_3$, this contact is longer [3.1898(3) Å], probably because of the greater bulkiness of the Bbt substituent.[22] The C−Te−O angle is almost linear in **2** and **3**, as well as in $[BbtTe(PPh_3)]O_3SCF_3$.[22]

The reaction of **1** with 2 equiv of Ph_3Sb produced the heteroleptic 1:1 LP complex $[MesTe(SbPh_3)][Ph_2Sb(O_3SCF_3)_2]$ (**4**), which features the cation $[MesTe(SbPh_3)]^+$ (**4a**) and the anion $[Ph_2Sb(O_3SCF_3)_2]^-$ (**4b**). Variation of the stoichiometry had no influence on the outcome of the reaction; e.g., no evidence for the formation of $[MesTe(SbPh_3)]O_3SCF_3$ was found. After removal of Mes_2Te, **4** was isolated by crystallization as a ruby-red solid in 46% yield (Scheme 2). The

Scheme 2. Synthesis of 4

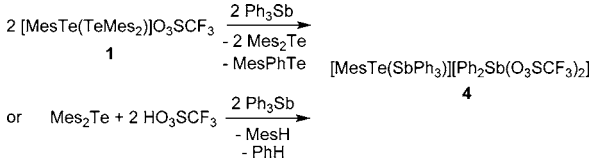

formation of the anion **4b** implies that a phenyl group migration from half of triphenylantimony to half of the mesityltellurenyl cation had occurred. The migration of aryl groups is not unprecedented in tellurium chemistry, which holds particularly true for mesityltellurium compounds.[14] The formation of the anion **4b** can be rationalized when the assumed Sb product of the phenyl group migration, $Ph_2SbO_3SCF_3$, reacted with additional triflate ions. The Te product of the phenyl group migration, the unsymmetrical diaryltelluride MesPhTe, was identified in the mother liquor by its ^{125}Te NMR chemical shift (419.7 ppm) after most of the Mes_2Te and **4** were removed by crystallization. To support the identification, MesTePh (a colorless oil), was independently prepared by the reaction of MesTeI (obtained in situ by the reaction of MesTeTeMes with iodine)[30] with PhMgBr. More efficiently, **4** was prepared by the one-pot reaction of Mes_2Te, Ph_3Sb, and HO_3SCF_3 and isolated in 92% yield.

The ^{125}Te NMR spectrum (CD_3CN) of **4** shows a signal at 418.4 ppm that is close to those of **1**−**3**. The ESI-MS spectrum (MeCN, positive and negative detection modes) of **4** exhibits the most intense mass clusters (except that for the triflate ion at m/z 148.6) at m/z 601.1 and 572.8 for the cation **4a** and the anion **4b**, respectively. The molar conductivity (MeCN, $c = 5 \times 10^{-7}$ mol L^{-1}) of **4** (Λ = 480 Ω^{-1} cm^2 mol^{-1}) is somewhat higher than those measured for **1** and **2**, accounting for the presence of 1:1 electrolytes. The molecular structure of **4** is shown in Figure 4, and selected bond parameters are collected in the caption of the figure. The molecular structure of **4a** closely resembles those of **2a** and **3a**. The Te−Sb bond lengths of **4a** [2.708(1) Å] compare well with the sum of covalent radii (2.77 Å).[28] In **2** and **3**, the triphenylpnictogens and triflate ions are situated in trans positions around the Te atoms (Figures 2 and 3). A similar arrangement was recently encountered within the 1:1 LP complex $[Cl_2Sb(AsMe_3)]O_3SCF_3$, in which Me_3As is situated in the trans position to the triflate ion.[31] In **4**, the cation **4a** interacts in the trans position with the π system of the mesityl group of an adjacent cation **4a** [closest distance Te1···C13b 3.501(3) Å]. A similar π interaction was recently observed for the 1:1 LP complex $[Cl_2Bi(SbPh_3)]AlCl_4$·toluene, in which the toluene molecule coordinates to the Bi atom in the trans position of Ph_3Sb.[32] In addition, **4** shows a contact between the cation **4a** and a triflate moiety of the anion **4b** in a side-on fashion. The related Te1···O2a [3.153(1) Å] and Sb1···O2a [3.106(3) Å] distances are shorter than the sum of van der Waals radii (3.58 and 3.64 Å, respectively). Owing to the stereochemically active lone pair at the Sb^{III} atom, the spatial arrangement of the Sb atom of the anion **4b** is trigonal-bipyramidal and defined by a C_2O_2 donor set for the primary coordination sphere, in which C and O atoms occupied the equatorial and axial positions, respectively.

In addition to the two primary Sb−O bonds, there are two secondary Sb···O contacts related to the two triflate moieties, completing the coordination sphere of the Sb. The Sb···O bond lengths [3.573(3) and 3.390(3) Å] are longer than the sum of covalent radii but significantly shorter than the sum of van der Waals radii (3.64 Å).[29] Interestingly, two cations **4a** are further associated with π stacking involving two phenyl rings and two mesityl rings that adopt nearly parallel conformations. The closest distance between the aryl rings is 3.268(6) Å for C11 and C35.

In the solid state, **1**−**4** possess an indefinite bench stability when stored at room temperature under argon. Compound **4** can even be handled in air for short periods of time, while the other compounds degrade rapidly. In solution, **1**−**4** are moderately stable and decompose under precipitation of Te powder. The relative stability decreases in the order **4** ≫ **1** > **2** ≫ **3**. The stability depends on the solvent and decreases in the order THF > MeCN > $CHCl_3$ ≈ CH_2Cl_2.

The reaction of **1** with 2 equiv of Ph_3Bi most likely provided the heteroleptic 1:1 LP complex $[MesTe(BiPh_3)][Ph_2Bi(O_3SCF_3)_2]$ (**5**), featuring the cation $[MesTe(BiPh_3)]^+$ (**5a**) and the anion $[Ph_2Bi(O_3SCF_3)_2]^-$ (**5b**), but could not be isolated in pure form (Scheme 3). The crude reaction mixture consisting of **5** was investigated immediately after removal of most Mes_2Te by crystallization and the solvent by vacuum evaporation. The ESI-MS spectrum (MeCN, positive detection mode) of **5** exhibits three intense mass clusters at m/z 363.1, 689.2, and 731.2 that were unambiguously assigned to the cations Ph_2Bi^+ (**6a**), **5a**, and $[Ph_2Bi(TeMes_2)]^+$, respectively. The ESI-MS spectrum (MeCN, negative detection mode) of **5** displays only one intense mass cluster at m/z 660.8 for the anion **5b**. The ^{125}Te NMR spectrum (CD_3CN) of crude **5**

dx.doi.org/10.1021/ic3017722 | Inorg. Chem. 2012, 51, 12395−12406

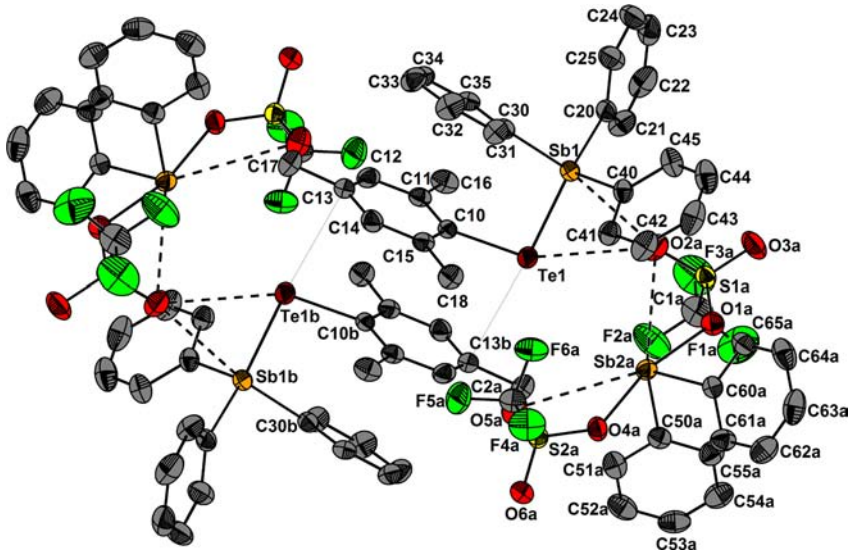

Figure 4. Molecular structure of **4** showing 50% probability ellipsoids and the crystallographic numbering scheme (symmetry codes used to generate crystallographically related atoms: a = *x*, 1 + *y*, *z*; b = 1 − *x*, −*y*, 1 − *z*). Selected bond parameters (Å and deg): Te1···O2a 3.156(3), Te1−Sb1 2.708(1), Te1−C10 2.125(3), Te1···C13b 3.501(3), Sb1···O2a 3.106(3), Sb1−C20 2.108(3), Sb1−C30 2.109(3), Sb1−C40 2.102(3), Sb2a−O1a 2.325(2), Sb2a···O2a 3.573(3), Sb2a−O4a 2.323(2), Sb2a···O5a 3.390(3), Sb2a−C50a 2.147(3), Sb2a−C60a 2.136(3); C10−Te1−Sb1 90.30(7), O1a−Sb2a−O4a 166.73(7), O1a−Sb2a−C50a 87.0(1), O1a−Sb2a−C60a 83.9(1), O4a−Sb2a−C50a 87.5(1), O4a−Sb2a−C60a 84.7(1), C50a−Sb2a−C60a 96.5(1).

Scheme 3. Attempted Synthesis of 5 and Synthesis of 6

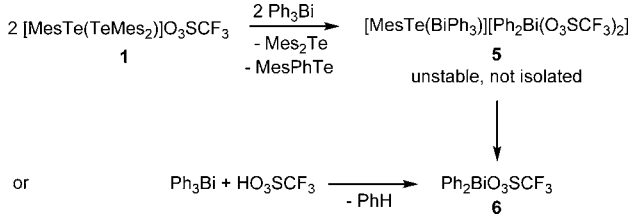

displays a main signal at δ 422.4 ppm, which matches well the ^{125}Te NMR chemical shifts observed for **2**−**4** (see above). Also visible was a minor signal at 250.5 ppm, which was assigned to Mes_2Te. No evidence was found for the 1:1 LP complex cation $[Ph_2Bi(TeMes_2)]^+$ by ^{125}Te NMR spectroscopy (see below). All attempts to isolate **5** by fractional crystallization failed but provided $Ph_2BiO_3SCF_3$ (**6**) as colorless crystals in 71% yield. The fact that the yield exceeds 50% suggests that not only the anion **5b** but also the cation **5a** are the sources of **6**. This is tentatively attributed to a degradation process involving phenyl group migration from Bi to Te within **5a**.

It is worth noting that similar aryl scrambling reactions between Bi and Te species are well-known and have been utilized for preparative purposes, e.g., the synthesis of diaryltellurides from triarylbismuth.[33] More rationally, **6** was obtained by the reaction of Ph_3Bi with triflic acid in 93% yield by a slightly modified literature procedure (Scheme 3).[34] We now add spectroscopic and structural details. Compound **6** is readily soluble in polar solvents such as MeCN, in which it undergoes electrolytic dissociation into **6a** and triflate ions. The molar conductivity (MeCN, $c = 5 \times 10^{-7}$ mol L^{-1}) of **6** (Λ = 460 Ω^{-1} cm^2 mol^{-1}) is consistent with the presence of 1:1 electrolytes. The ESI-MS spectra (MeCN, positive and negative detection modes) of **6** show only intense mass clusters at *m*/*z* 363.1 and 660.8, belonging to the cation **6a** and the anion **5b**, respectively. Interestingly, when a solution of **6** in MeCN was exposed to the atmosphere for 1 h prior to the measurement, the ESI-MS spectrum also reveals a mass cluster at *m*/*z* 379.1, which was assigned to the cation $[Ph_2Bi(O)]^+$ (**6b**), which apparently formed by air oxidation of **6a**. The crystal structure of **6** is shown in Figure 5, and selected bond parameters of **6** are

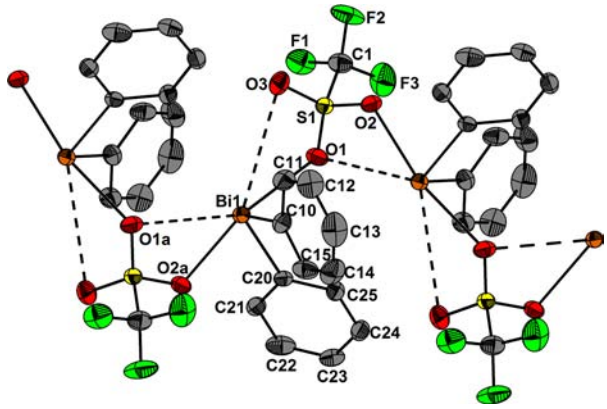

Figure 5. Crystal structure of **6** showing 50% probability ellipsoids and the crystallographic numbering scheme (symmetry code used to generate crystallographically related atoms: a = −1 − *x*, −1 − *y*, 0.5 + *z*). Selected bond parameters (Å and deg): Bi1−O1 2.531(6), Bi1···O1a 3.480(6), Bi1−O2a 2.473(5), Bi1···O3 3.553(6), Bi1−C10 2.233(7), Bi1−C20 2.223(7); O1−Bi1−O2a 168.5(2), O1−Bi1−C10 86.2(2), O1−Bi1−C20 86.5(2), O2a−Bi1−C10 88.6(2), O2a−Bi1−C20 84.0(2), C10−Bi1−C20 97.2(3).

collected in the caption of the figure. It comprises a 1D polymer containing sequences of ion-paired cations **6a** and triflate anions. Bearing in mind the stereochemically active lone pair, the spatial arrangement of the Bi atoms is trigonal-bipyramidal, whereby the first coordination sphere is defined by a C_2O_2 donor set. The primary Bi−O bond lengths of **6** [2.473(5) and 2.531(6) Å] are slightly longer than those of 2,6-(*t*-BuO)$_2$C$_6$H$_3$Bi(O$_3$SCF$_3$)$_2$ [2.389(7) and 2.393(6) Å].[35] There are also two secondary Bi···O contacts [3.480(6) and

dx.doi.org/10.1021/ic3017722 | *Inorg. Chem.* 2012, 51, 12395−12406

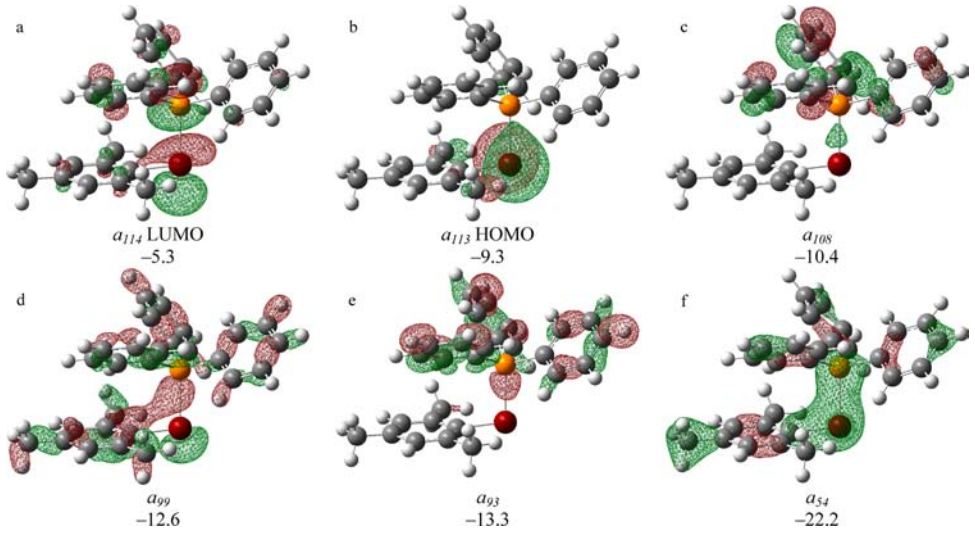

Figure 6. MO isosurface plots (0.04 au densities) of **2a** and corresponding energies (eV).

3.553(6) Å], completing the coordination sphere of the Bi atom of **6**. In an effort to prepare the 1:1 LP complex $[Ph_2Bi(TeMes_2)]O_3SCF_3$, the NMR scale reaction of **6** and Mes_2Te was carried out in CD_3CN at room temperature, the ^{125}Te NMR spectrum of which shows only the presence of Mes_2Te. Attempts to isolate a 1:1 LP complex by fraction crystallization afforded crops of the reactants. In contrast to the heteroleptic 1:1 and 1:2 LP complexes $[Ph_2Bi(PPh_3)_n]PF_6$ (n = 1, 2),[5−8] the desired 1:1 LP complex $[Ph_2Bi(TeMes_2)](O_3SCF_3)$ is apparently not favored in the solid state.

DFT Calculations and NBO, AIM, and ELI-D Analyses. Like the homo- and heteroleptic group 15 LP complexes $[R_2E(E'R_3')_n]^+$ (E, E′ = P, As, Sb, Bi; R, R′ = alkyl, aryl; n = 1, 2),[1,3−8] the bismesityltelluride-stabilized mesityltellurenyl cation **1a** and the triphenylpnictogen-stabilized mesityltellurenyl cations $[MesTe(EPh_3)]^+$ (**2a**, E = P; **3a**, E = As; **4a**, E = Sb) are archetypical examples of p-block compounds comprising formal dative bonds, which makes them worthwhile candidates for detailed bond analyses.

To get a deeper insight into the bond situation, single-point calculations of the cationic 1:1 LP complexes **1a**−**4a** were performed on the DFT level of theory. The (vertical) bond dissociation energies of the complexes increases in the order **1a** (243.4 kJ mol^{-1}) < **4a** (289.3 kJ mol^{-1}) < **3a** (303.4 kJ mol^{-1}) < **2a** (322.6 kJ mol^{-1}). These energies are in the same order of magnitude as the dissociation energy of the fully optimized 1:1 LP complex $[PhTe(PMe_3)]^+$ (328.6 kJ mol^{-1}) published in our preceding work.[19] The homoleptic 1:1 LP complex **1a** has the lowest dissociation energy, which is consistent with the results of the substitution experiments, leading to the formation of the more stable heteroleptic 1:1 LP complexes $[MesTe(EPh_3)]^+$ (**2a**, E = P; **3a**, E = As; **4a**, E = Sb). Characteristic MOs of **1a** and $[MesTe(EPh_3)]^+$ (**2a**, E = P; **3a**, E = As; **4a** E = Sb) were visualized, and a representative selection of **2a** is shown in Figure 6. The MOs of **1a**, **3a**, and **4a** are of similar shape and energy (see S4 in the Supporting Information). For all four 1:1 LP complexes, the highest occupied molecular orbital (HOMO) is a p-like lone pair situated at the Te cation and the lowest unoccupied molecular orbital is comprised of an antibonding combination of p orbitals at the donor atoms E (E = Te, P, As, Sb) and the acceptor atom Te (Figure 6a,b and S4 in the Supporting Information). Because of strong electron delocalization involving the aryl groups, no single MO for the Te−E bond was found. Instead, there are a number of MOs indicating the binding character of the Te−E bond. These were analyzed by orbital contribution analysis of the corresponding disynaptic ELI-D bonding basins and canonical molecular orbital (CMO) analysis according to the NBO scheme.

Analysis of the electron density (ED) distribution provides complementary information to quantum-mechanical-based approaches and empirical bonding schemes like the valence-shell electron-pair repulsion model. The ED is an observable and can thus, in principle, not only be calculated but also obtained experimentally by high-resolution X-ray diffraction at low temperatures and subsequent asperical atom refinement, e.g., based on the Hansen−Coppens multipole formalism.[36] An ED obtained by either calculation or experiment can be analyzed topologically by the AIM theory[37] of Bader, which by the introduction of surfaces of zero electron flux generates atomic basins and enables a straightforward quantitative interpretation of atomic and bonding properties. This approach has been applied to a large number of chemical systems in the last 2 decades.[38,39] The molecular or crystalline ED of any given assemblage of atoms typically exhibits bond paths [and related bond critical points (bcp's)] linking adjacent atoms. In covalently bonded systems, these bond paths unambiguously correspond to the molecular graph, which intuitively would be drawn by chemists.

Moreover, bond paths are found for all types of chemical interactions, including ionic, metallic, and intermolecular hydrogen-bonded and van der Waals bonded systems. However, for multicenter-bonded systems like supported metal carbonyls and clusters of main-group elements like boranes, this one-to-one relationship is not valid anymore.[40,41] Becuase of this, further bond descriptors that do not rely on the existence of bcp's are required. Integrated bonding descriptors like the delocalization index $[\delta(x,y)]$,[42,43] which is a measure of the electron sharing between two atoms, are not sensitive to the topology. Moreover, parallel to ED analysis, different types of localization functions appeared, which divide space into regions of localized electron pairs instead of atoms and therefore greatly complement the AIM theory. The ELI-D[44] applied here is a further development of the prominent electron localization function (ELF).[45,46] To the best of our knowledge, there is only

Table 1. Topological Bond Descriptors[a]

	$\rho(r_{bcp})$ [e Å^{-3}]	$\nabla^2\rho(r_{bcp})$ [e Å^{-5}]	d [Å]	d_1 [Å]	d_2 [Å]	ε	$G/\rho(r_{bcp})$ [h e^{-1}]	$H/\rho(r_{bcp})$ [h e^{-1}]
MesTe$^+$: Te−C								
	0.71	0.0	2.133	1.099	1.034	0.07	0.52	−0.51
Mes$_2$Te: Te−C								
	0.71	−0.3	2.140	1.103	1.038	0.10	0.49	−0.52
Ph$_3$E: E−C								
E = P	0.97	−5.8	1.832	0.733	1.099	0.16	0.60	−0.98
E = As	0.85	−2.3	1.954	0.946	1.008	0.08	0.49	−0.66
E = Sb	0.67	1.4	2.149	1.083	1.066	0.06	0.61	−0.48
LP Complex: Te−E								
1a	0.39	−0.1	2.807	1.456	1.355	0.21	0.30	−0.31
2a	0.54	−0.8	2.481	1.224	1.257	0.25	0.34	−0.43
3a	0.48	−0.5	2.580	1.272	1.308	0.23	0.31	−0.38
4a	0.44	−0.4	2.708	1.350	1.358	0.26	0.31	−0.36
LP Complex: Te−C								
1a	0.72	−0.6	2.133	1.111	1.022	0.04	0.46	−0.52
2a	0.74	−0.6	2.114	1.101	1.012	0.02	0.47	−0.53
3a	0.73	−0.7	2.123	1.107	1.016	0.02	0.46	−0.52
4a	0.72	−0.7	2.124	1.110	1.015	0.03	0.46	−0.52
LP Complex: E−C								
1a	0.74	−1.3	2.132	1.122	1.010	0.10	0.42	−0.53
2a	1.05	−7.8	1.804	0.738	1.066	0.11	0.51	−1.01
3a	0.92	−3.5	1.921	0.956	0.965	0.09	0.43	−0.67
4a	0.73	0.5	2.107	1.083	1.024	0.08	0.56	−0.51

[a]For all bonds, $\rho(r_{bcp})$ is the ED at the bcp; $\nabla^2\rho(r_{bcp})$ is the corresponding Laplacian; d is the distance of the two bonded nuclei, d_1 and d_2 are the distances from atoms x and y to the bcp; ε is the bond ellipticity [$\varepsilon = (\lambda_1/\lambda_2) - 1$; $\lambda_1 > \lambda_2$]; $G/\rho(r_{bcp})$ and $H/\rho(r_{bcp})$ are the kinetic and total energy densities over ρ ratios, respectively.

one report utilizing ELI-D in tellurium chemistry, namely, to describe the bond situation in the complex $Te_{10}[Ir(TeCl_4)(TeCl_3)]_2$.[47] For both ELF and ELI-D, the partitioning follows the same rules as those used by AIM to separate atoms from each other. Thus, it is space-filling and discrete, providing reliable integrated electron numbers of both core shells and (non)bonded valence electrons. Valence basins connecting two core basins are called disynaptic, whereas lone pairs and H atoms exhibit so-called (protonated) monosynaptic valence basins. The disadvantage of ELF, not comparable between different molecules because localization is always related to the uniform electron gas of the very same compound, was discarded with the introduction of ELI-D. The bond topological properties of **1a**−**4a** are collected in Table 1 and reveal all occurring bond types (C−E and Te−E; E = P, As, Sb, Te) to be of polar covalent nature. Representations of the ELI-D basins of **1a**−**4a** are shown in Figure 7

The ED at the bcp's lies between 0.39 e Å^{-3} (the polar covalent Te−Te bond of **1a**) and 1.05 e Å^{-3} (the mainly covalent P−C bonds of **2a**), with all Laplacians being slightly negative, which is a sign of covalency, or almost zero. The covalency is also reflected in the negative value of the total energy over the density ratio $H/\rho(r_{bcp})$, which is again the largest for the P−C bonds. In the line P, As, Sb, and Te, the $\rho(r_{bcp})$ values of all C−E and Te−E bonds show a trend of decreasing density, which is essentially related to the increasing bond lengths. Upon complex formation, all E−C (E = P, As, Sb) and Te−C bonds become shorter, thus leading to higher $\rho(r_{bcp})$ values. The large bond ellipticities of the Te−E bonds (0.21−0.25) reflect their diffuse and delocalized nature.

In terms of AIM partitioning, the positive charge of the free mesityltellurenyl cation is to 61% located at the Te atom (Table 2); the rest is evenly distributed over the mesityl group (see

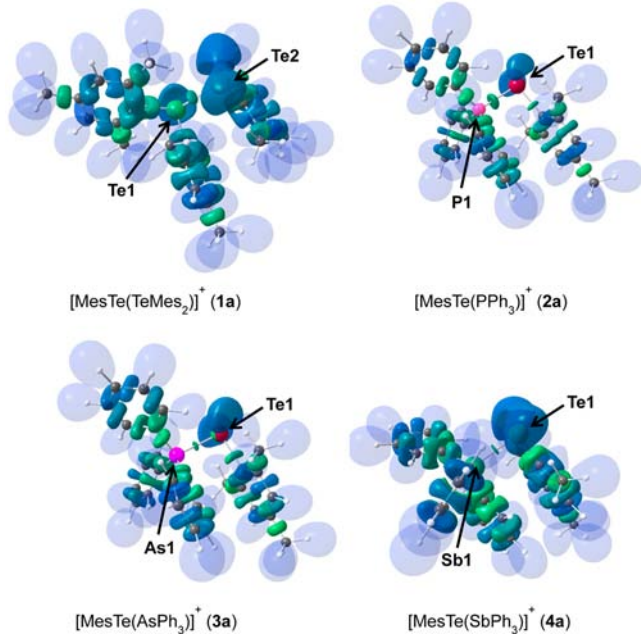

Figure 7. ELI-D of **1a** (γ = 1.30), **2a** (γ = 1.50), **3a** (γ = 1.40), and **4a** (γ = 1.30).

part S5.1 in the Supporting Information). In the uncharged free donor molecules, there is also a pronounced internal charge polarization, in that the donor atoms E are significantly positive (0.47 e, E = Te; 1.51 e, E = P; 0.93 e, E = As; 1.12 e, E = Sb) and the aryl substituents are negative. Interestingly, Ph_3As does not follow the trend suggested by the results for P, Sb, and Te, which is attributed to the influence of the filled 3d shell. Upon LP complex formation, 0.67−0.83 e are transferred from Ph_3E

dx.doi.org/10.1021/ic3017722 | Inorg. Chem. 2012, 51, 12395−12406

Table 2. AIM Net Charges (e)[a]

	R−E	E	Te$^+$	Te−R	$\sum R_{3/2}$−E	$\sum$TeMes
Single Components						
MesTe$^+$			0.61	0.39		1.00
Mes_2Te	−0.24	0.47			0.00	
Ph_3P	−0.50	1.51			0.00	
Ph_3As	−0.31	0.93			0.00	
Ph_3Sb	−0.37	1.12			0.00	
LP Complexes						
1a	−0.05	0.83	0.36	−0.09	0.72	0.27
2a	−0.35	1.72	0.42	−0.10	0.67	0.33
3a	−0.12	1.08	0.38	−0.09	0.72	0.28
4a	−0.18	1.39	0.26	−0.09	0.83	0.17

[a]The AIM net charges are the difference of the integrated number of electrons within the zero flux surface, $\oint_{x \cap y'}$ around the atom and electrons of the isolated atom.

(E = P, As, Sb) to the mesityltellurenyl cation. This leads to a less positive Te atom of the cation (0.26−0.42 e instead of 0.61 e) and a slightly negative mesityl group (ca. −0.1 e instead of 0.39 e); see Table 2 for details. As expected, the phenyl groups of the triphenylpnictogens Ph_3E become less negative upon complex formation, while the donor atoms E = Te, P, As, Sb become even more positively charged (electron loss of about 0.2−0.3 e), which leads to a strong charge polarization between the Te atom of the cation and the donating atoms and concomitantly to polar covalent Te−Te and Te−E bonds. This is essentially in accordance with the bond topological properties.

The integrated bond properties (Table 3) give a detailed view of the charge redistributions upon complex formation and complement analysis of the topological bond properties and atomic charges. The free mesityltellurenyl cation MesTe$^+$ stabilizes its charge by exhibiting an electronic structure, which may be described as partially quinoid: Te═(C−C/C′═C/C′−C)$_{ring}$. The Te═C double-bond character is reflected in large values for δ(Te,C) = 1.44 and ELI-D population = 2.30 e, compared to 1.02 and 1.91 e in Mes_2Te. The results for the mesityl group are given in part S6.2 of the Supporting Information. Upon complex formation, the Te−C bond becomes a single bond and the mesityl fragment recovers its aromatic character (see Scheme S7 in the Supporting Information). The two nonbonding electron pairs of the Te atom of the mesityltellurenyl cation MesTe$^+$ behave unexpectedly. Instead of gaining charge from the donor molecules, they each (slightly) lose 0.02 e (**1a**) to 0.14 e (**2a**). The charge donation from Lewis base to the cation is most clearly visible in the significant decrease of the electron population within the former lone pairs of the Te, P, As, and Sb atoms of free Mes_2Te and Ph_3E (E = P, As, Sb). These electron-pair basins are connecting Lewis acid and base comprising the Te−E bond. The charge depletion becomes more and more dominant with increasing size of the donor atom E (0.70 e, E = Te; 0.16 e, E = P; 0.37 e, E = As; 0.44 e, E = Sb). Because the initial electron population also increases in the series P, As, and Sb, the Te−E bonds (E = P, As, Sb) show quite similar bond characteristics. The Te−Te bond is an exception with a very small electron population of 1.61 e compared to 1.89−1.95 e for Te−E bonds (E = P, As, Sb). This is presumably due to the influence of the second lone pair of the Mes_2Te donor, which upon complex formation carries the large amount of 2.60 e. This lets us surmise that stabilization of the mesityltellurenyl cations may be tuned with the electron donors not only by variation of the donor atom type but also by different numbers of nonbonding electron pairs at the donor atom. As the E−C bonds (E = P, As, Sb, Te) of the donor molecules become shorter upon complex formation (see above), they gain small amounts of charge (0.1−0.25 e). For estimation of the bond polarities of the Te−E bonds, the quite new concept of overlapping ELI-D valence basins with AIM atoms is helpful, which is expressed by the Jansen index J.[48] For homopolar bonds, e.g., the C−C bond in ethane, the electrons within the C−C bonding basin are to 50% located within each C atom; thus, J = 50%. With increasing bond polarity, one finds an increasing amount of electron populations located within the more electronegative atom (J > 50%). With this concept, one can discriminate polar covalent interactions (50% < J < 95%) from dative bonds (J > 95%), and by quantification of the ED in the ELI-D basin parts, it allows a reliable estimation of the charge transfer between Lewis base and acid.[49] The Jansen index J confirms that all listed bond types are polar covalent, because all relative electron populations lie within the boundaries of 50% and 95% (Table 3). Moreover, it shows that all bonds are less polar upon complex formation because all values come closer to 50%. For the E−C bonds of the donor molecules, this effect is more pronounced than that for the Te−C bond of the cation.

In **2a**, orbital contribution analysis of the Te−P ELI-D basin shows that the ED of this basin stems mainly from the MOs a_{54}, a_{99}, a_{87}, a_{93}, a_{102}, and a_{111} (12.0, 10.0, 9.7, 7.2, 7.0, and 6.5%, respectively; Figure 6c−f). CMO analysis shows larger contributions of the Te−P bonding NBO to MOs a_{99}, a_{54}, a_{87}, a_{102}, and a_{93} (13.2, 10.2, 10.1, 7.1, and 5.5%, respectively). While in orbital a_{54}, the ED is equally distributed around the Te−P bond, the orbitals a_{111}, a_{102}, a_{93}, and a_{87} show EDs along the Te−P bond mostly concentrated toward the P atom, resembling the lone pair of the triphenylphosphine moiety. Orbital a_{99} shows a π interaction of the MesTe$^+$ unit with a deformed p-like orbital at the P atom, which could be interpreted as π-back-donation of the lone pair at the tellurium to the donor. In addition, MO a_{108} reflects a nonpolar covalent binding with the ED equally distributed between the two atoms (but this orbital corresponds only to 3.4% to the Te−P basin). For the LP complexes **3a** and **4a** and with minor limitations also **1a**, orbitals with comparable shape and energy could also be found (see S4 in the Supporting Information, for example), so that, in summary, the bonding situation in all of these complexes could be described as polar covalent. The overall MO interpretation of these complexes is in good comparison with that described for the 1:1 LP complexes $[Ph_2E(PPh_3)]^+$ (E = P, As, Sb, Bi).[8]

CONCLUSIONS

Starting from simple reactants [e.g., Mes_2Te, Ph_3E (E = P, As, Sb) and HO_3SCF_3], the 1:1 LP complexes **1**−**4** were prepared and fully characterized. Compounds **1**−**4** comprise the archetypical σ-donor-stabilized mesityltellurenyl cations **1a** and $[MesTe(EPh_3)]^+$ (**2a**, E = P; **3a**, E = As; **4a**, E = Sb) containing polar covalent Te−E bonds (E = Te, P, As, Sb), which have been analyzed by DFT calculations and analysis methods, including NBO, AIM, and ELI-D. These show that most of the positive charge is situated at the donor atoms E, which, in fact, suggests that the complexes are best described as telluronium (**1a**), phosponium (**2a**), arsonium (**3a**), and stibonium cations (**4a**). The HOMOs of **1a**−**4a** are p-like lone pairs situated at the mesityltellurenyl cations. We are

dx.doi.org/10.1021/ic3017722 | Inorg. Chem. 2012, 51, 12395−12406

Table 3. Integrated Bond Descriptors[a]

	$\delta(x,y)$	ELI-D_{pop} [e]	V_{001}^{ELI} [Å^{-3}]	ELI_{max} γ	Δ_{ELI} [Å]	pop_1	pop_2	J_2 [%]
$MesTe^+$								
LP1		2.40	17.8	1.83				
LP2		2.40	18.5	1.90				
Mes_2Te								
LP1		2.31	16.7	1.80				
LP2		2.31	16.9	1.84				
Ph_3E: LP E								
E = P		2.05	16.5	2.67				
E = As		2.31	18.5	2.29				
E = Sb		2.39	23.0	2.10				
Ph_3E: E−C								
E = P	0.84	2.14	4.9	1.89	0.059	0.459	1.679	78.5
E = As	0.91	2.14	5.4	1.77	0.069	0.658	1.478	69.2
E = Sb	0.86	2.15	7.0	1.75	0.044	0.526	1.623	75.4
Mes_2Te								
Te−C	1.01	1.91	5.1	1.65	0.079	0.546	1.362	71.0
$MesTe^+$								
Te−C	1.44	2.30	10.6	1.59	0.012	0.696	1.605	69.8
LP Complexes: Lone Pairs at Te								
1a, LP1		2.39	17.1	1.75				
1a, LP2		2.37	17.6	1.82				
1a, LP Mes_2Te		2.60	18.1	1.78				
2a, LP1		2.25	15.0	1.75				
2a, LP2		2.27	15.2	1.73				
3a, LP1		2.30	15.6	1.75				
3a, LP2		2.31	15.8	1.74				
4a, LP1		2.32	15.9	1.72				
4a, LP2		2.33	16.3	1.71				
LP Complexes: Te−E								
1a	0.98	1.61	5.8	1.36	0.270	0.448	1.156	71.9
2a	0.95	1.89	6.5	1.72	0.056	0.550	1.339	70.8
3a	0.95	1.94	7.3	1.44	0.045	0.502	1.432	73.8
4a	0.97	1.95	9.7	1.32	0.138	0.577	1.276	65.4
LP Complexes: Te−C								
1a	1.04	1.93	5.2	1.60	0.010	0.633	1.294	67.1
2a	1.04	1.92	5.1	1.60	0.019	0.640	1.279	66.6
3a	1.05	1.90	5.0	1.60	0.017	0.639	1.260	66.3
4a	1.05	1.87	4.8	1.59	0.012	0.636	1.232	65.9
LP Complexes: E−C								
1a	0.96	1.97	5.2	1.60	0.090	0.795	1.169	59.4
2a	0.84	2.24	5.5	1.89	0.012	0.630	1.608	71.8
3a	0.90	2.23	6.0	1.71	0.020	0.910	1.317	59.1
4a	0.85	2.23	7.9	1.66	0.031	0.779	1.447	65.0

[a]For all bonds, $\delta(x,y)$ is the delocalization index of atoms x and y; ELI-D_{pop} is the electron population of the ELI-D basins; V_{001}^{ELI} is the corresponding volume cut at an ED value of 0.001 au; ELI_{max} γ is the corresponding ELI-D value at the attractor position; Δ_{ELI} is the distance of the attractor position perpendicular to the xy axis; pop_1 and pop_2 are the absolute numbers of electrons of an ELI-D basin within an AIM atom, respectively, and J_2 is the Jansen index, which is given relative to pop_2.

currently exploring the possibility of utilizing **1**−**4** as electron-pair donors for the synthesis of transition-metal complexes.[50] For instance, preliminary work has shown that the reaction of **4** with $Fe(CO)_5$ gives rise to a crude product, the ESI-MS spectrum (MeCN, positive detection mode) of which shows a mass cluster at m/z 769.0, which was assigned to the cation $[MesTe(SbPh_3)(Fe(CO)_4)]^+$ based on the correct isotopic pattern. Similar "push−pull" complexes were recently reported for NHC-stabilized silylenes,[51] germylenes,[52,53] and stannylenes.[53]

EXPERIMENTAL SECTION

General Procedures. The starting material Mes_2Te [$\delta(^{125}Te)$ = 250.5 ppm][54] was prepared according to literature procedures, whereas Ph_3E (E = P, As, Sb, Bi) and triflic acid were obtained commercially and used as received. The ^1H, ^{13}C, and ^{125}Te NMR spectra were recorded at room temperature (unless otherwise stated) using a Bruker Avance-360 spectrometer and are referenced to $SiMe_4$ (^1H and ^{13}C), 85% H_3PO_4 (^{31}P), and Me_2Te (^{125}Te). As secondary references, solutions of 100 mg samples of Ph_2Se_2 [$\delta(^{77}Se)$ = 464.0 ppm] in $CDCl_3$ and $Te(OH)_6$ [$\delta(^{125}Te)$ = 707.0 ppm] in D_2O were used. The ESI-MS spectra were obtained with a Bruker Esquire-LC ion-trap mass spectrometer. Acetonitrile solutions (c = 1 × 10^{-6} mol L^{-1}) were injected directly into the spectrometer at a flow rate of 3 μL

dx.doi.org/10.1021/ic3017722 | Inorg. Chem. 2012, 51, 12395−12406

min^{-1}. Nitrogen was used both as a drying gas and for nebulization with flow rates of approximately 5 L min^{-1} and a pressure of 5 psi, respectively. The pressure in the mass analyzer region was usually about 1×10^{-5} mbar. Spectra were collected for 1 min and averaged. The nozzle−skimmer voltage was adjusted individually for each measurement. Elemental analyses were obtained using a HEKAtech Euro EA-CHNS analyzer. Because of the limited stability, reasonable results were obtained only for **4**. All conductivity measurements have been carried out with a WTW Cond 330i at 25 °C.

Synthesis of $[MesTe(TeMes_2)]O_3SCF_3$ (1). To a continuously stirred suspension of Mes_2Te (1.00 g, 2.73 mmol) in dry CH_3CN (60 mL) was slowly added triflic acid (0.21 g, 1.37 mmol). The deep-red solution was stirred overnight and the solvent as well as residual acid removed under reduced pressure. Crystallization (CH_2Cl_2/*n*-hexane) afforded **1** as brownish dark-red crystals (0.91 g, 1.19 mmol, 87%; dec at 168 °C without melting).

^1H NMR (CD_3CN): δ 7.07 (s, 2H), 7.01 (s, 4H), 2.23 (s, 9H), 2.13 (s, 18H). ^1H NMR ($CDCl_3$): δ 6.95 (s, 2H), 6.90 (s, 4H), 2.30 (s, 9H), 2.17 (s, 18H). $^{13}C\{^1H\}$ NMR (CD_3CN): δ 149.1, 144.6, 144.3, 144.2, 138.7, 131.5, 129.2, 127.8, 119.2, 118.4, 30.5, 25.6, 21.3, 21.2, 20.9. $^{13}C\{^1H\}$ NMR ($CDCl_3$): δ 148.2, 143.7, 143.5, 142.1, 138.0, 130.2, 128.6, 127.2, 119.9, 118.0, 30.2, 26.4, 21.3, 21.2, 21.0. ^{125}Te NMR (CD_3CN): δ 932.1 ($\omega_{1/2}$ = 222 Hz), 396.3. ^{125}Te NMR ($CDCl_3$): δ 844.8 ($\omega_{1/2}$ = 293 Hz), 376.5. ESI-MS (CH_3CN, positive mode): *m*/*z* 617.2 ($C_{27}H_{33}Te_2$) for $MesTe(TeMes_2)]^+$ (**1a**). Molar conductivity (CH_3CN, $c = 5 \times 10^{-7}$ mol L^{-1}): Λ = 360 Ω^{-1} cm^2 mol^{-1}.

Synthesis of $[MesTe(PPh_3)]O_3SCF_3$ (2). Method A. To a solution of **1** (0.95 g, 1.25 mmol) in dry CH_3CN (30 mL) was added Ph_3P (0.33 g, 1.25 mmol). The orange solution was stirred for 72 h, precipitated Mes_2Te (0.09 g, 0.25 mmol) was filtered off, and the solvent was removed under reduced pressure. Crystallization (CH_2Cl_2/*n*-hexane) afforded **2** as orange crystals (0.65 g, 0.99 mmol, 79%; mp 76 °C). **Method B.** Mes_2Te (0.50 g, 1.36 mmol) and Ph_3P (0.36 g, 1.36 mmol) were dissolved in dry CH_3CN (35 mL), and triflic acid (0.20 g, 1.36 mmol) was slowly added. The orange solution was stirred for 24 h, and the solvent was removed under reduced pressure. Crystallization (CH_2Cl_2/*n*-hexane) afforded **2** as orange crystals (0.69 g, 1.00 mmol, 77%; mp 76 °C).

^1H NMR (CD_3CN): δ 7.76 (m, 3H), 7.60 (m, 12H), 6.87 (s, 2H), 2.29 (s, 3H), 2.19 (s, 6H). ^1H NMR ($CDCl_3$): δ 7.69 (t, 3H), 7.51 (m, 6H), 7.36 (m, 6H), 6.81 (s, 2H), 2.22 (s, 3H), 2.13 (s, 6H). $^{13}C\{^1H\}$ NMR (CD_3CN): δ 147.8, 143.5, 135.6, 135.0 (d, $^2J(^{13}C-^{31}P)$ = 11.4 Hz), 130.9 (d, $^3J(^{13}C-^{31}P)$ = 12.7 Hz), 129.3, 128.7, 127.6, 117.3, 29.9, 21.0. $^{13}C\{^1H\}$ NMR ($CDCl_3$): δ 147.1, 142.7, 135.0 (d, $^1J(^{13}C-^{31}P)$ = 1.7 Hz), 133.7 [d, $^2J(^{13}C-^{31}P)$ = 5.3 Hz], 130.1 (d, $^3J(^{13}C-^{31}P)$ = 6.5 Hz), 128.6, 120.2, 119.5, 114.9, 29.3, 20.9. $^{31}P\{^1H\}$ NMR (CD_3CN): δ 4.7. $^{31}P\{^1H\}$ NMR ($CDCl_3$): δ 6.0. ^{125}Te NMR (CD_3CN): δ 385.6 ($\omega_{1/2}$ = 185 Hz). ^{125}Te NMR ($CDCl_3$): δ 393.0 ($^1J(^{125}Te-^{31}P)$ = 1148 Hz). ESI-MS (CH_3CN, positive mode): *m*/*z* 511.1 ($C_{27}H_{26}PTe$) for $[MesTe(PPh_3)]^+$ (**2a**). Molar conductivity (CH_3CN, $c = 5 \times 10^{-7}$ mol L^{-1}): Λ = 400 Ω^{-1} cm^2 mol^{-1}.

Synthesis of $[MesTe(AsPh_3)]O_3SCF_3$ (3). Method A. To a solution of **1** (0.95 g, 1.25 mmol) in diethyl ether (30 mL) was added Ph_3As (0.38 g, 1.25 mmol). The orange solution was stirred for 72 h, precipitated Mes_2Te was filtered off, and the solvent was removed under reduced pressure. Crystallization (diethyl ether/*n*-hexane) afforded **3** as orange crystals (0.23 g, 0.33 mmol, 26%). **Method B.** Mes_2Te (0.50 g, 1.36 mmol) and Ph_3As (0.42 g, 1.36 mmol) were dissolved in dry diethyl ether (35 mL), and triflic acid (0.20 g, 1.36 mmol) was slowly added. The orange solution was stirred for 24 h and the solvent removed under reduced pressure. Crystallization (CH_2Cl_2/*n*-hexane) afforded **3** as orange crystals (0.21 g, 0.30 mmol, 22%).

^1H NMR (CD_3CN): δ 7.62 (m, 3H), 7.46 (m, 12H), 6.82 (s, 2H), 2.32 (s, 6H), 2.22 (s, 3H). $^{13}C\{^1H\}$ NMR (CD_3CN): δ 147.8, 143.5, 138.6, 133.9, 133.8, 131.0, 129.1, 128.7, 127.7, 127.1, 30.6, 21.2. ^{125}Te NMR (CD_3CN): δ 408.5. ^{125}Te NMR ($CDCl_3$): δ 414.8. ESI-MS (CH_3CN, positive mode): *m*/*z* 555.2 ($C_{27}H_{26}AsTe]^+$ for $[MesTe(AsPh_3)]^+$ (**3a**).

Synthesis of $[MesTe(SbPh_3)][Ph_2Sb(O_3SCF_3)_2]$ (4). Method A. To a solution of **1** (0.95 g, 1.25 mmol) in dry CH_3CN (30 mL) was added Ph_3Sb (0.44 g, 1.25 mmol). The red solution was stirred for 72 h, precipitated Mes_2Te was filtered off, and the solvent was removed under reduced pressure. Crystallization (CH_2Cl_2/*n*-hexane) afforded **4** as red crystals (0.68 g, 0.58 mmol, 46%; mp 122−125 °C). **Method B.** Mes_2Te (0.50 g, 1.36 mmol) and Ph_3Sb (0.95 g, 2.70 mmol) were dissolved in CH_3CN (35 mL), and triflic acid (0.41 g, 2.70 mmol) was slowly added. The red solution was stirred for 24 h and the solvent removed under reduced pressure. Crystallization (CH_2Cl_2/*n*-hexane) afforded **4** as ruby-red crystals (1.47 g, 1.25 mmol, 92%; mp 122−125 °C).

^1H NMR (CD_3CN): δ 7.54 (m, 6H), 7.46 (m, 17H), 6.84 (m, 4H), 2.45 (s, 6H), 2.34 (s, 3H). $^{13}C\{^1H\}$ NMR (CD_3CN): δ 147.5, 145.0, 138.6, 136.6, 136.1, 133.2, 131.2, 131.0, 130.0, 129.3, 128.9, 128.7, 127.7, 127.3, 31.4, 21.2. ^{125}Te NMR (CD_3CN): δ 418.4. ^{125}Te NMR ($CDCl_3$): δ 425.5. ESI-MS (CH_3CN, positive mode): *m*/*z* 601.1 $[C_{27}H_{26}SbTe]^+$ for $[MesTe(SbPh_3)]^+$ (**4a**). ESI-MS (CH_3CN, negative mode): *m*/*z* 572.8 $[C_{14}H_{10}F_6O_6S_2Sb]^-$ for **4b**. Molar conductivity (CH_3CN, $c = 5 \times 10^{-7}$ mol L^{-1}): Λ = 480 Ω^{-1} cm^2 mol^{-1}. Anal. Calcd for $[MesTe(SbPh_3)]^+[Ph_2Sb(O_3SCF_3)_2]^-$, 1176.96: C, 41.95; H, 3.09; S, 5.46. Found: C, 42.08; H, 3.38; S, 5.18.

Synthesis of MesTePh. A solution of MesTeI [freshly prepared by the addition of solid iodine (1.02 g, 8.04 mmol) to a solution of $(MesTe)_2$ (1.97 g, 4.00 mmol) in toluene (30 mL), which was allowed to react for 1h] was treated with a solution of phenylmagnesium bromide [prepared from bromobenzene (1.26 g, 8.03 mmol) and activated Mg turnings (0.26 g, 10.69 mmol) in THF (30 mL)]. The solution was stirred overnight and then quenched with a Na_2SO_3 solution (10%, 20 mL). The organic layer was separated and dried over Na_2SO_4.

After removal of the solvent in vacuum, the crude product was purified by column chromatography (silica/*n*-hexane) to give MesTePh as a colorless oil (1.61 g, 4.98 mmol, 62%).

^1H NMR ($CDCl_3$): δ 7.31 (2H, m), 7.13 (3H, m), 7.00 (2H, s), 2.52 (6H, s), 2.32 (3H, s). $^{13}C\{^1H\}$ NMR ($CDCl_3$): δ 145.4, 139.4, 134.6, 129.4, 127.6, 126.6, 118.3, 116.3, 29.4, 21.0. ^{125}Te NMR ($CDCl_3$): δ 419.7.

Attempted Synthesis of $[MesTe(BiPh_3)][Ph_2Bi(O_3SCF_3)_2]$ (5). To a solution of **1** (0.95 g, 1.25 mmol) in dry CH_3CN (30 mL) was added Ph_3Bi (0.55 g, 1.25 mmol). The yellow solution was stirred for 48 h, precipitated Mes_2Te removed by filtration, and the solvent removed under reduced pressure.

^{125}Te NMR (CD_3CN): δ 422.4. ^{125}Te NMR ($CDCl_3$): δ 414.2. ESI-MS (CH_3CN, positive mode): *m*/*z* 731.2 $[C_{30}H_{32}BiTe]^+$ for $[Ph_2Bi(TeMes_2)]^+$, 689.2 $[C_{27}H_{26}BiTe]^+$ for $[MesTeBiPh_3]^+$ (**5a**), 363.1 $[C_{12}H_{10}Bi]^+$ for $[Ph_2Bi]^+$ (**6a**). ESI-MS (CH_3CN, negative mode): *m*/*z* 660.8 $[C_{14}H_{10}BiF_6O_6S_2]^-$ for $[Ph_2Bi(O_3SCF_3)_2]^-$ (**5b**).

Crystallization (CH_2Cl_2/*n*-hexane) afforded **6** as colorless crystals (0.41 g, 0.88 mmol, 71%; dec at 152 °C without melting).

Synthesis of $Ph_2BiO_3SCF_3$ (6). A solution of Ph_3Bi (2.20 g, 5.00 mmol) in CH_2Cl_2 (50 mL) was cooled to −78 °C, and triflic acid (0.75 g, 5.00 mmol) was added. After the solution was stirred for 10 min at low temperature, it was warmed to room temperature and stirred for another 10 h. Quick evaporation of the solvent afforded a white solid, which was recrystallized from CH_3CN to yield **6** as colorless crystals (2.38 g, 4.65 mmol, 93%; dec at 152 °C without melting).

^1H NMR (CD_3CN): δ 8.45 (d, 4H), 7.82 (t, 4H), 7.48 (t, 2H). $^{13}C\{^1H\}$ NMR (CD_3CN): δ 139.2, 133.6, 130.0. ESI-MS (CH_3CN, positive mode): *m*/*z* 363.1 $[C_{12}H_{10}Bi]^+$ for $[Ph_2Bi]^+$ (**6a**). ESI-MS (CH_3CN, negative mode): *m*/*z* 660.8 $[C_{14}H_{10}BiF_6O_6S_2]^-$ for **5b**. Molar conductivity (CH_3CN, $c = 5 \times 10^{-7}$ mol L^{-1}): Λ = 460 Ω^{-1} cm^2 mol^{-1}.

X-ray Crystallography. Intensity data were collected on a STOE IPDS 2T area detector (**1**) and a Siemens P4 diffractometer (**2**−**4** and **6**) fitted with a Siemens LTII at 173 K with graphite-monochromated Mo Kα (0.7107 Å) radiation. All structures were solved by direct methods and refined based on F^2 by use of the *SHELX* program package.[55] All non-H atoms were refined using anisotropic displace-

ment parameters. H atoms attached to C atoms were included in geometrically calculated positions using a riding model. Crystal and refinement data are collected in Table S1 in the Supporting Information. Figures were created using *DIAMOND*.[56] Crystallographic data (excluding structure factors) for the structural analyses have been deposited with the Cambridge Crystallographic Data Centre, CCDC 886605 (**1**), 886606 (**2**), 886607 (**3**), 886608 (**4**), and 886609 (**6**). Copies of this information may be obtained free of charge from The Director, CCDC, 12 Union Road, Cambridge CB2 1EZ, U.K. (fax +44-1223-336033; e-mail deposit@ccdc.cam.ac.uk, or http://www.ccdc.cam.ac.uk).

Computational Methodology. Single-point calculations of the cationic complexes **1a**, **2a**, **3a**, and **4a** applying the DFT/B3PW91[57] functional were performed using the crystallographic geometry with the program package *Gaussian09*.[58] For Te and Sb atoms, an ECP28MDF electron core potential and the appropriate cc-pVTZ basis set were applied; for all other atoms, the 6-311+G(2df,p) basis set was used.[59] Calculations of the donors, Mes_2Te,[60] Ph_3P,[61] Ph_3As,[62] and Ph_3Sb[63] were equally performed using the structural data taken from the CCDC database. If there was more than one symmetry-inequivalent molecule in the unit cell, one representative was chosen (for coordinates, see the Supporting Information). The structure of the isolated $MesTe^+$ cation was taken from complex **1**. C−H distances of all substances were set to neutron diffraction data (C_{sp^2}−H 1.083 Å; C_{sp^3}−H 1.059 Å) prior to processing.[64] NBO analyses were performed using *NBO 5.9*.[65] For the AIM analyses, wave function files were generated along with single-point calculations and analyzed using AIMAll.[66] DGrid was used to analyze the ELI-D, revealing the integrated bond descriptors using a 0.05 au grid and a 3.0 au box around the molecule.[67] Figures of the ELI-D were generated with the program *MolIso*.[68]

■ ASSOCIATED CONTENT

Supporting Information

Crystal data and structure refinement of compounds **1**−**4** and **6** as well as details of the computations including geometries, total energies, MO plots for compounds **1a**−**4a**, detailed AIM charges and integrated bond descriptors, plots of the ELI-D, and a comparison of the delocalization indices and the ELI-D population of the mesityl fragment in the complexes. This material is available free of charge via the Internet at http://pubs.acs.org.

■ AUTHOR INFORMATION

Corresponding Author

*E-mail: j.beckmann@uni-bremen.de (J.B.), stebs@chemie.fu-berlin.de (S.M.). Tel.: ++49(0)421 218-63160. Fax: ++49(0) 421 218-9863160.

Notes

The authors declare no competing financial interest.

■ DEDICATION

†Dedicated to Professor Rüdiger Mews on the occasion of his 70th birthday.

■ REFERENCES

(1) (a) Burford, N.; Cameron, T. S.; Ragogna, P. J. *J. Am. Chem. Soc.* **2001**, *123*, 7947−7948. (b) Burford, N.; Rogogna, P. J.; McDonald, R.; Ferguson, M. J. *J. Am. Chem. Soc.* **2003**, *125*, 14404−14410.
(2) Kuhn, N.; Fahl, J.; Bläser, D.; Boese, R. *Z. Anorg. Allg. Chem.* **1999**, *625*, 729−734.
(3) Kilah, N. L.; Weir, M. L.; Wild, S. B. *Dalton Trans.* **2008**, 2480−2486.
(4) Althaus, H.; Breunig, H. J.; Lork, E. *Chem. Commun.* **1999**, 1971−1972.
(5) Porter, K. A.; Willis, A. C.; Zank, J.; Wild, S. B. *Inorg. Chem.* **2002**, *41*, 6380−6386.
(6) Burford, N.; Ragogna, P. J.; Sharp, K.; McDonald, R.; Ferguson, M. J. *Inorg. Chem.* **2005**, *44*, 9453−9460.
(7) Wielandt, J. W.; Kilah, N. L.; Willis, A. C.; Wild, S. B. *Chem. Commun.* **2006**, 3679−3680.
(8) Kilah, N. L.; Petrie, S.; Stranger, R.; Wielandt, J. W.; Willis, A. C.; Wild, S. B. *Organometallics* **2007**, *26*, 6106−6113.
(9) (a) Sato, S.; Ameta, H.; Horn, E.; Takahasi, O.; Furukawa, N. *J. Am. Chem. Soc.* **1988**, *110*, 1280−1284. (b) Fujihara, H.; Mima, H.; Erata, T.; Furukawa, N. *J. Am. Chem. Soc.* **1992**, *114*, 3117−3118. (c) Bergholdt, A. B.; Kobayashi, K.; Horn, E.; Takahashu, O.; Sato, S.; Furukawa, N.; Yokoyama, M.; Yamaguchi, K. *J. Am. Chem. Soc.* **1998**, *120*, 1230−1236. (d) Kobayashi, K.; Sato, S.; Horn, E.; Furukawa, N. *Angew. Chem., Int. Ed.* **2000**, *39*, 1318−1320.
(10) (a) Dutton, J. L.; Tuononen, H. M.; Jennings, M. C.; Ragogna, P. J. *J. Am. Chem. Soc.* **2006**, *128*, 12624−12625. (b) Martin, C. D.; Le, C. M.; Ragogna, P. J. *J. Am. Chem. Soc.* **2009**, *131*, 15126−15127. (c) Martin, C. D.; Jennings, M. C.; Ferguson, M. J.; Ragogna, P. J. *Angew. Chem., Int. Ed.* **2009**, *48*, 2210−2213. (d) Martin, C. D.; Ragogna, P. J. *Inorg. Chem.* **2010**, *49*, 4324−4330. (e) Martin, C. D.; Ragogna, P. J. *Inorg. Chem.* **2010**, *49*, 8164−8172. (f) Dutton, J. L.; Ragogna, P. *Chem.—Eur. J.* **2010**, *16*, 12454−12461. (g) Martin, C. D.; Ragogna, P. J. *Inorg. Chem.* **2012**, *49*, 2947−2953. (h) Dube, J. W.; Hänninen, M. M.; Dutton, J. L.; Tuononen, H. M.; Ragogna, P. J. *Inorg. Chem.* **2012**, DOI: 10.1021/ic300892p.
(11) Fujihara, H.; Mima, H.; Furukawa, N. *J. Am. Chem. Soc.* **1995**, *117*, 10153−10154.
(12) Beleaga, A.; Bojan, V. R.; Pöllnitz, A.; Rat, C.; Silvestru, C. *Dalton Trans.* **2011**, *40*, 8830−8838.
(13) Jeske, J.; du Mont, W.-W.; Jones, P. G. *Angew. Chem., Int. Ed.* **1997**, *36*, 2219−2221.
(14) Jeske, J.; du Mont, W.-W.; Ruthe, F.; Jones, P. G.; Mercuri, L. M.; Deplano, P. *Eur. J. Inorg. Chem.* **2000**, 1591−1599.
(15) Hrib, C. G.; Jeske, J.; Jones, P. G.; du Mont, W.-W. *Dalton Trans.* **2007**, 3483−3485.
(16) Köllemann, C.; Sladky, F. *J. Organomet. Chem.* **1990**, *396*, C1−C3.
(17) Imrie, C.; Modro, T. A.; van Rooyen, P. H.; Wagener, C. C. P.; Wallace, K.; Hudson, H. R.; McPartlin, M.; Nasirun, J. B.; Powroznyk, L. *J. Phys. Org. Chem.* **1995**, *8*, 41−46.
(18) Jones, P. G.; Thöne, C. *Z. Kristallogr.* **1994**, *209*, 78−79.
(19) Beckmann, J.; Finke, P.; Heitz, S.; Hesse, M. *Eur. J. Inorg. Chem.* **2008**, 1921−1925.
(20) Poleschner, H.; Seppelt, K. *Angew. Chem., Int. Ed.* **2008**, *47*, 6461−6464.
(21) (a) Huang, X.; Batchelor, R. J.; Einstein, F. W. B.; Bennet, A. J. *J. Org. Chem.* **1994**, *59*, 7108−7116. (b) Lucchini, V.; Modena, G.; Pasi, M.; Pasquato, L. *J. Chem. Soc., Chem. Commun.* **1994**, 1565−1566. (c) Lucchini, V.; Modena, G.; Pasi, M.; Pasquato, L. *J. Org. Chem.* **1997**, *62*, 7018−7020. (d) Wirth, T.; Fragale, G.; Spichty, M. *J. Am. Chem. Soc.* **1998**, *120*, 3376−3381. (e) Fachini, M.; Lucchini, V.; Modena, G.; Pasi, M.; Pasquato, L. *J. Am. Chem. Soc.* **1999**, *121*, 3944−3950. (f) Uehlin, L.; Fragale, G.; Wirth, T. *Chem.—Eur. J.* **2002**, *8*, 1125−1133. (g) Denmark, S. E.; Collins, W. R.; Cullen, M. D. *J. Am. Chem. Soc.* **2009**, *131*, 3490−3492. (h) Denmark, S. E.; Vogler, T. *Chem.—Eur. J.* **2009**, *15*, 11737−11745. (i) Denmark, S. E.; Kalyani, D.; Collins, W. R. *J. Am. Chem. Soc.* **2010**, *132*, 15752−15765.
(22) Sugamata, K.; Sasamori, T.; Tokitoh, N. *Eur. J. Inorg. Chem.* **2012**, 775−778.
(23) (a) Chivers, T.; Konu, J.; Ritch, J. S.; Copsey, M. C.; Eisler, D. J.; Tuononen, H. M. *J. Organomet. Chem.* **2007**, *692*, 2658−2668. (b) Ritch, J. S.; Chivers, T. *Dalton Trans.* **2008**, 957−962. (c) Robertson, S. D.; Chivers, T. *Dalton Trans.* **2008**, 1765−1772. (d) Robertson, S. D.; Chivers, T.; Tuononen, H. M. *Inorg. Chem.* **2008**, *47*, 10634−10643. (e) Robertson, S. D.; Chivers, T.; Tuononen, H. M. *Dalton Trans.* **2009**, 8582−8592. (f) Ritch, J. S.; Chivers, T. *Inorg. Chem.* **2009**, *48*, 3857−3865. (g) Robertson, S. D.; Chivers, T.;

Tuononen, H. M. *Inorg. Chem.* **2009**, *48*, 6755−6762. (h) Konu, J.; Tuononen, H. M.; Chivers, T. *Inorg. Chem.* **2009**, *48*, 11788−11798.
(24) Zhao, H.; Gabbaï, F. P. *Nat. Chem.* **2010**, *2*, 984−990.
(25) Lin, T.-P.; Gabbaï, F. P. *J. Am. Chem. Soc.* **2012**, *134*, 12230−12238.
(26) (a) Schmeißer, M.; Sartori, P.; Lippsmeier, B. *Chem. Ber.* **1970**, *103*, 868−879. (b) Bassindale, A. R.; Stout, T. *J. Organomet. Chem.* **1984**, *271*, C1−C3. (c) Uhlig, W. *J. Organomet. Chem.* **1991**, *402*, C45−C49. (d) Uhlig, W. *J. Organomet. Chem.* **1991**, *409*, 377−383. (e) Uhlig, W. *Trends Organomet. Chem.* **1997**, *2*, 1−19.
(27) Geary, W. J. *Coord. Chem. Rev.* **1971**, *7*, 81−122.
(28) Cordero, B.; Gómez, V.; Platero-Prats, A. E.; Revés, M.; Echeverría, J.; Cremades, E.; Barragán, F.; Alvarez, S. *Dalton Trans.* **2008**, 2832−2838.
(29) Bondi, A. *J. Phys. Chem.* **1964**, *68*, 441−451.
(30) (a) Ledesma, G. N.; Schulz Lang, E.; Vázquez-López, E. M.; Abram, U. *Inorg. Chem. Commun.* **2004**, *7*, 478−480. (b) Hrib, C. G.; Jones, P. G.; du Mont, W.-W.; Lippolis, V.; Devillanova, F. A. *Eur. J. Inorg. Chem.* **2006**, 1294−1302. (c) Faoro, E.; Manzoni de Oliveira, G.; Schulz Lang, E. *J. Organomet. Chem.* **2006**, *691*, 5867−5872. (d) Faoro, E.; Manzoni de Oliveira, G.; Schulz Lang, E.; Bicca Pereira, C. *J. Organomet. Chem.* **2011**, *696*, 2438−2444.
(31) Conrad, E.; Burford, N.; McDonald, R.; Ferguson, M. J. *J. Am. Chem. Soc.* **2009**, *131*, 5066−5067.
(32) Conrad, E.; Burford, N.; McDonald, R.; Ferguson, M. J. *Chem. Commun.* **2010**, *46*, 4598−4600.
(33) Arnauld, T.; Barton, D. H. R.; Normant, J.-F. *J. Org. Chem.* **1999**, *64*, 3722−3725.
(34) Labrouillere, M.; Le Roux, C.; Gaspard, H.; Laporterie, A.; Dubac, J. *Tetrahedron Lett.* **1999**, *40*, 285−286.
(35) Dostál, L.; Novák, P.; Jambor, R.; Růžička, A.; Císařová, I.; Jirásko, R.; Holeček, J. *Organometallics* **2007**, *26*, 2911−2917.
(36) Hansen, N. K.; Coppens, P. *Acta Crystallogr.* **1978**, *A34*, 909−921.
(37) Bader, R. F. W. *Atoms in Molecules. A Quantum Theory*; Cambridge University Press: Oxford U.K., 1991.
(38) Koritsanszky, T.; Coppens, P. *Chem. Rev.* **2001**, *101*, 1583−1628.
(39) Gatti, C. *Z. Kristallogr.* **2005**, 399−457.
(40) Ponec, R.; Gatti, C. *Inorg. Chem.* **2009**, *48*, 11024−11031.
(41) Mebs, S.; Kalinowski, R.; Grabowsky, S.; Förster, D.; Kickbusch, R.; Justus, E.; Morgenroth, W.; Paulmann, C.; Luger, P.; Gabel, D.; Lentz, D. *Inorg. Chem.* **2011**, *50*, 90−103.
(42) Bader, R. F. W.; Stephens, M. E. *J. Am. Chem. Soc.* **1975**, *97*, 7391−7399.
(43) Fradera, X.; Austen, M. A.; Bader, R. F. W. *J. Phys. Chem. A* **1999**, *103*, 304−314.
(44) Kohout, M. *Int. J. Quantum Chem.* **2004**, *97*, 651−658.
(45) Becke, A. D.; Edgecombe, K. E. *J. Chem. Phys.* **1990**, *92*, 5397−5403.
(46) Silvi, B.; Savin, A. *Nature* **1994**, *371*, 683−686.
(47) Günther, A.; Heise, M.; Wagner, F. R.; Ruck, M. *Angew. Chem.* **2011**, *123*, 10163−10167.
(48) (a) Raub, S.; Jansen, G. *Theor. Chem. Acc.* **2001**, *106*, 223−232. (b) Vidal, I.; Melchor, S.; Dobado, J. A. *J. Phys. Chem. A* **2005**, *109*, 7500−7508.
(49) (a) Mebs, S.; Grabowsky, S.; Förster, D.; Kickbusch, R.; Hartl, M.; Daemen, L. L.; Morgenroth, W.; Luger, P.; Paulus, B.; Lentz, D. *J. Phys. Chem. A* **2010**, *114*, 10185−10196. (b) Mebs, S.; Kalinowski, R.; Grabowsky, S.; Förster, D.; Kickbusch, R.; Justus, E.; Morgenroth, W.; Paulmann, C.; Luger, P.; Gabel, D.; Lentz, D. *J. Phys. Chem. A* **2011**, *115*, 1385−1395.
(50) Torubaev, Y.; Pasynskii, A.; Mathur, P. *Coord. Chem. Rev.* **2012**, *256*, 709−721.
(51) (a) Ghadwal, R. S.; Azhakar, R.; Pröpper, K.; Holstein, J. J.; Dittrich, B.; Roesky, H. W. *Inorg. Chem.* **2011**, *50*, 8502−8508. (b) Al-Rafia, S. M. I.; Malcom, A. C.; McDonald, R.; Ferguson, M. J.; Rivard, E. *Chem. Commun.* **2012**, *48*, 1308−1310.
(52) Thimer, K. C.; Al-Rafia, S. M. I.; Ferguson, M. J.; McDonald, R.; Rivard, E. *Chem. Commun.* **2009**, 7119−7121.
(53) Al-Rafia, S. M. I.; Malcom, A. C.; Liew, S. K.; Ferguson, M. J.; Rivard, E. *J. Am. Chem. Soc.* **2011**, *133*, 777−779.
(54) Lederer, K. *Ber. Deutsch. Chem. Ges.* **1916**, *49*, 345−349.
(55) Sheldrick, G. M. *Acta Crystallogr.* **2008**, *A64*, 112−122.
(56) *Diamond—Crystal and Molecular Structure Visualization, Crystal Impact*; K. Brandenburg & H. Putz GbR: Bonn, Germany.
(57) (a) Perdew, J. P.; Chevary, J. A.; Vosko, S. H.; Jackson, K. A.; Pederson, M. R.; Singh, D. J.; Fiolhais, C. *Phys. Rev. B* **1992**, *46*, 6671−6687. (b) Becke, A. D. *J. Chem. Phys.* **1993**, *98*, 5648−5652.
(58) Frisch, M. J.; Trucks, G. W.; Schlegel, H. B.; Scuseria, G. E.; Robb, M. A.; Cheeseman, J. R.; Scalmani, G.; Barone, V.; Mennucci, B.; Petersson, G. A.; Nakatsuji, H.; Caricato, M.; Li, X.; Hratchian, H. P.; Izmaylov, A. F.; Bloino, J.; Zheng, G.; Sonnenberg, J. L.; Hada, M.; Ehara, M.; Toyota, K.; Fukuda, R.; Hasegawa, J.; Ishida, M.; Nakajima, T.; Honda, Y.; Kitao, O.; Nakai, H.; Vreven, T.; Montgomery, J. A., Jr.; Peralta, J. E.; Ogliaro, F.; Bearpark, M.; Heyd, J. J.; Brothers, E.; Kudin, K. N.; Staroverov, V. N.; Kobayashi, R.; Normand, J.; Raghavachari, K.; Rendell, A.; Burant, J. C.; Iyengar, S. S.; Tomasi, J.; Cossi, M.; Rega, N.; Millam, J. M.; Klene, M.; Knox, J. E.; Cross, J. B.; Bakken, V.; Adamo, C.; Jaramillo, J.; Gomperts, R.; Stratmann, R. E.; Yazyev, O.; Austin, A. J.; Cammi, R.; Pomelli, C.; Ochterski, J. W.; Martin, R. L.; Morokuma, K.; Zakrzewski, V. G.; Voth, G. A.; Salvador, P.; Dannenberg, J. J.; Dapprich, S.; Daniels, A. D.; Farkas, Ö.; Foresman, J. B.; Ortiz, J. V.; Cioslowski, J.; Fox, D. J. *Gaussian09*, revision B.01; Gaussian, Inc.: Wallingford, CT, 2009.
(59) (a) Peterson, K. A.; Figgen, D.; Goll, E.; Stoll, H.; Dolg, M. *J. Chem. Phys.* **2003**, *119*, 11113−11123. (b) Metz, B.; Stoll, H.; Dolg, M. *J. Chem. Phys.* **2000**, *113*, 2563−2569. (c) Peterson, K. A. *J. Chem. Phys.* **2003**, *119*, 11099−11112.
(60) Klapötke, T. M.; Krumm, B.; Mayer, P.; Polhorn, K.; Schwab, I. *Z. Anorg. Allg. Chem.* **2005**, *631*, 2677−2682.
(61) Kooijman, H.; Spek, A. L.; van Bommel, K. J. C.; Verboom, W.; Reinhoudt, D. N. *Acta Crystallogr.* **1998**, *C54*, 1695−1698.
(62) Sobolev, A. N.; Belsky, V. K.; Chernikova, N. Yu.; Akhmadulina, F. Yu. *J. Organomet. Chem.* **1983**, *244*, 129−136.
(63) Adams, E. A.; Kolis, J. W.; Pennington, W. T. *Acta Crystallogr.* **1990**, *C46*, 917−919.
(64) Wilson, A. J. C. *International Tables of Crystallography*; Kluwer Academic Publishers: Boston, 1992; Vol. *C*.
(65) Glendening, E. D.; Badenhoop, J. K.; Reed, A. E.; Carpenter, J. E.; Bohmann, J. A.; Morales, C. M.; Weinhold, F. *NBO*, version 5.0; Theoretical Chemistry Institute, University of Wisconsin, Madison, WI, 2001.
(66) Keith, T. A. *AIMAll*, version 11.09.18; TK Gristmill Software: Overland Park, KS, 2011.
(67) Kohout, M. *DGrid*, version 4.5/4.6; Radebeul, Germany, 2011.
(68) Hübschle, C. B.; Luger, P. *J. Appl. Crystallogr.* **2006**, *39*, 901−904.